BREHM + MULLIN

Example

Oxygen, sulfur, and selenium occur in the same column of the periodic table at $Z = 8$, 16, and 34. The ground-state configurations describe an unfilled p subshell with two electron vacancies in each case:

O	S	Se
$[He]2s^2 2p^4$	$[Ne]3s^2 3p^4$	$[Ar]4s^2 3d^{10} 4p^4$

These elements can fill their vacancies by accepting electrons from two hydrogen atoms to form the molecules H_2O, H_2S, and H_2Se. The two vacant sites in O, S, and Se have angular probability distributions characteristic of an $\ell = 1$ subshell. We can interpret the three m_ℓ assignments for $\ell = 1$ in terms of large distributions of probability along three perpendicular directions. Therefore, we expect to find right-angle shapes when we attach two H atoms to O, S, and Se to make the three triatomic molecules. This expectation is borne out since the hydrogen bonds are at angles of 105°, 93°, and 90° in H_2O, H_2S, and H_2Se. (The angle tends to exceed 90° because of Coulomb repulsion between the two hydrogens and approaches 90° in the largest molecule where the repulsion is weakest.)

9-4 X-Ray Spectra

The periodic table organizes the states of electrons outside closed subshells as the basis for the low-energy regularities of atoms. The underlying shell theory also governs the *inner* shells of the atom where the electrons engage in higher-energy processes such as the emission of x rays. This inner-shell behavior can be examined in a given atom by analyzing an x-ray spectrum like the one shown in Figure 9-8. We have discussed the production of x rays in Section 2-6, and we have taken a preliminary look at characteristic x rays as a source of inner-electron information in Section 3-7. We now return to the study of x-ray spectra with a proper quantum theory at our disposal and find that the independent-electron model provides an especially suitable approach.

Let us reconsider our previous picture of x-ray emission in Figure 9-3 and visualize the excitation and deexcitation of the system from the viewpoint presented in Figure 9-9. The revised picture describes these processes in terms of the single-electron energy levels in the central-field model. We represent the collisional excitation of the atom by the creation of a vacancy, or *hole*, in one of the fully occupied inner subshells. The

Figure 9-8
X-ray lines in the K and L series of tungsten. The heights of the lines are indicative of the observed intensities. The $K\alpha_1$ line at 0.0209100 nm is used to define an x-ray wavelength standard.

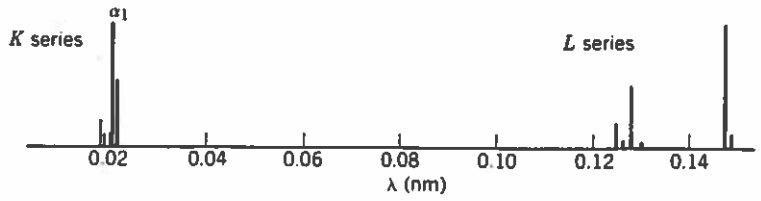

Figure 9-9
Excitation and deexcitation processes associated with x-ray emission.

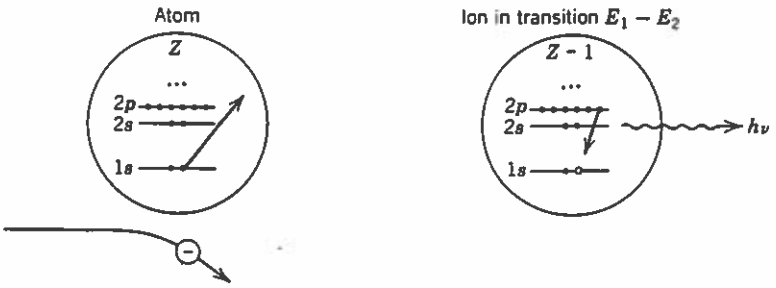

result is the formation of a highly excited ionic state with initial energy E_1. We then represent the radiative deexcitation of the system by letting an electron from a higher subshell fill the hole and emit an x-ray photon. The emitted photon has energy

$$h\nu = E_1 - E_2, \tag{9-11}$$

where E_2 is the energy of the excited final state in which the vacancy appears in the higher subshell. Observe from the figure that the x-ray transition occurs in the *ion* containing $Z - 1$ electrons. Note especially that a vacancy in a higher-energy subshell corresponds to a *lower* energy state of the ion, so that a hole stands for an *absence* of energy, as well as charge, in the overall electron system.

Let us also consider the related quantum phenomenon of x-ray absorption. This process is an example of the familiar photoelectric effect, where the absorption of an x-ray photon excites the atom above its ionization level and ejects a bound electron. A quantum mechanical probability can be introduced to describe the photon–atom interaction, and an absorption cross section can be defined to account for the behavior of a beam of x rays incident on the atoms in a sample of matter. We measure absorption in the laboratory by observing the attenuation of an x-ray beam in its passage through a thickness of material. The fractional decrease in intensity $-dI/I$ is related to the element of thickness dx by the proportionality

$$-\frac{dI}{I} = \mu_x\, dx,$$

where the constant μ_x defines the absorption coefficient of the material. This expression is easily integrated to give the intensity as a function of distance x through the sample, starting with incident intensity I_0:

$$\int_{I_0}^{I} \frac{dI}{I} = -\int_0^x \mu_x\, dx \quad \Rightarrow \quad \ln\frac{I}{I_0} = -\mu_x x \quad \Rightarrow \quad I = I_0 e^{-\mu_x x}.$$

The absorption coefficient varies with the material and depends on the wavelength of the x rays. We can use measurements of the attenuation to determine this dependence, and we can then infer the related behavior of the absorption cross section for the given element.

Figure 9-10
K and L absorption edges of lead. The wavelength thresholds occur where the x-ray photon energy becomes insufficient to eject a K- or L-shell electron. Emission lines of lead in the K and L series are also shown.

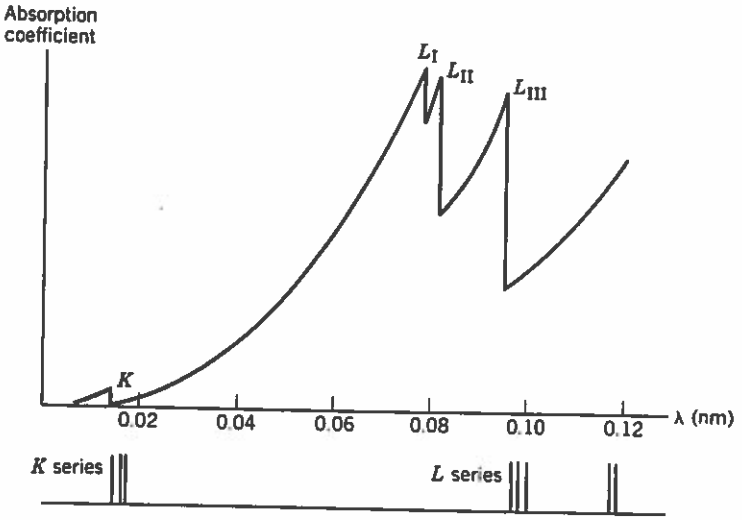

Figure 9-10 shows a typical graph of μ_x as a function of the wavelength λ. We observe zero absorption in the limit $\lambda \to 0$. This observation tells us that the absorbing medium is transparent to x rays when the beam energy is very large. We then observe a steady growth in absorption as the photon energy decreases from large values and as λ increases from zero, until we reach a sharp value of λ where the medium suddenly becomes transparent again. This feature of the graph is called an *absorption edge*, the first of several to appear with increasing λ in the figure. The indicated K absorption edge occurs at wavelength λ_K, where the photon energy is the minimum needed to ionize the atom and leave a vacancy in the K shell. When λ becomes larger than λ_K, the x-ray photon energy becomes too small to free a K-shell electron but remains large enough to eject an electron from an L (or higher) shell. We again observe a steady growth in absorption as the wavelength continues to increase until we reach one of the indicated L absorption edges. The various absorption thresholds are tabulated along with the characteristic x-ray emission lines. Both features provide a signature of the particular atom, and both give an indication of the energy levels of the system. We include the emission lines of the K and L series in the figure so that we can note the positions of these spectral lines relative to the absorption edges.

X-ray absorption can be interpreted with the aid of our representation of the atom as a collection of occupied subshells. Figure 9-11 describes the process in these terms at two different wavelength thresholds. The wavelengths λ_1 and λ_2 correspond to photons whose energies just suffice to eject an electron with no kinetic energy from the particular subshells shown in the figure. We leave the excited ion in states of energy E_1 and E_2 in the two cases, and we note the relation

$$E_1 > E_2 \quad \text{for} \quad \lambda_1 < \lambda_2.$$

Figure 9-11
X-ray absorption processes at two different absorption edges.

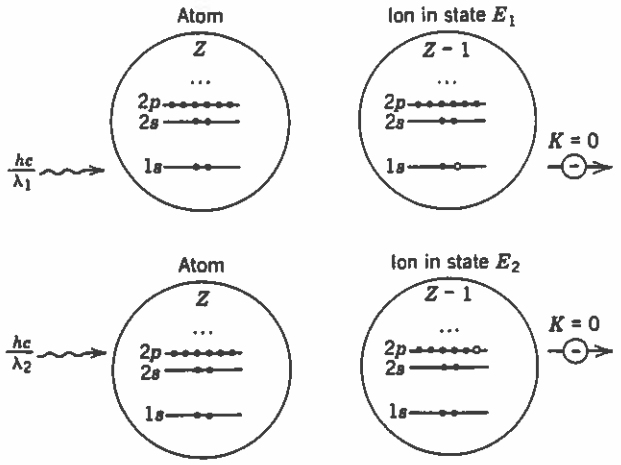

The figure tells us that the wavelengths and energies obey the formulas

$$\frac{hc}{\lambda_1} = E_1 - E_{\text{atom}} \quad \text{and} \quad \frac{hc}{\lambda_2} = E_2 - E_{\text{atom}}, \tag{9-12}$$

where E_{atom} denotes the energy of the initial atom. If we compare Figures 9-9 and 9-11, we see that the two ionic energies are the same as the energies E_1 and E_2 in Equation (9-11). If we combine Equations (9-11) and (9-12), we establish the following connection between x-ray absorption and x-ray emission:

$$h\nu = \frac{hc}{\lambda_1} - \frac{hc}{\lambda_2}. \tag{9-13}$$

This formula relates the wavelengths for two absorption edges to the frequency for a certain emission line in the spectrum of a given element. The equality implies an inequality of the form

$$\frac{hc}{\lambda} < \frac{hc}{\lambda_1} \quad \text{or} \quad \lambda > \lambda_1$$

for an emitted x ray of wavelength $\lambda = c/\nu$. This observation explains why the lines in a given series have wavelengths *above* the corresponding absorption edge, as indicated in Figure 9-10.

The absorption and emission of x rays reveal a new problem that requires an amendment to the central-field model. Figure 9-10 shows the existence of *three* L absorption edges instead of the two expected for the $2s$ and $2p$ subshells in the L shell. This behavior is a clear indication that the $n\ell$ assignments of the model are not adequate to describe the energy levels of the independent electrons. The effect is reminiscent of the multiplet structure of the one-electron atom and is attributable to a

Figure 9-12
Single-electron subshells including the effect of spin–orbit coupling.

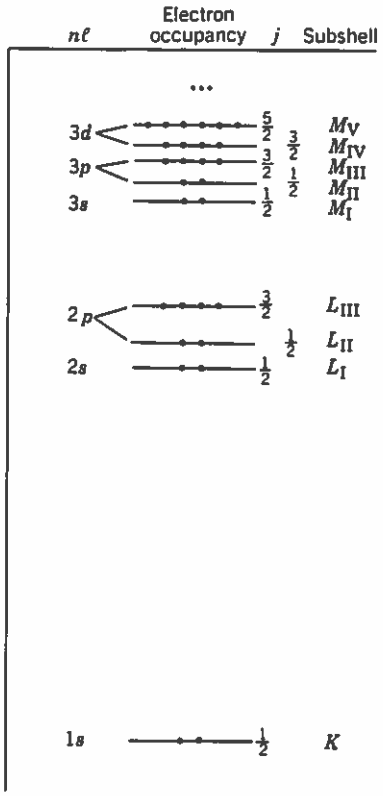

Figure 9-13
X-ray emission associated with the transition $K \rightarrow L_{III}$. An electron in the L_{III} subshell fills a vacancy in the K shell while the hole makes a transition from K to L_{III}. The standard $K\alpha_1$ line of tungsten corresponds to this transition.

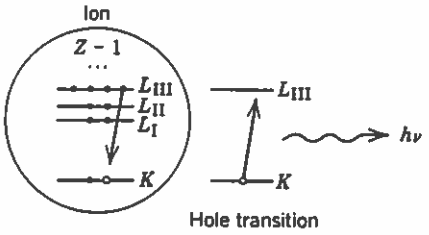

spin–orbit coupling experienced by each electron in addition to its interaction with the central field. We discuss some of the details of this coupling at the end of the section.

Figure 9-12 shows how these considerations alter the independent-electron picture of the atom by the introduction of the quantum number j. We let each energy level with subshell quantum numbers n and ℓ be *split* for $\ell \neq 0$ in the manner of Figure 8-28, and we recall the familiar quantum numbers $(n\ell jm_j)$ to specify the new single-electron states. We also label the energy levels by the *x-ray spectroscopic notation*

$$K \quad L_I\, L_{II} L_{III} \quad M_I\, M_{II}\, M_{III} M_{IV} M_V \quad \cdots$$

according to the tabulation given in the figure. The exclusion principle is built into this new scheme of states by stipulating that no two electrons are allowed to have the same four quantum numbers $(n\ell jm_j)$. Hence, each of the split $n\ell j$ subshells has a maximum occupancy equal to $2j + 1$, corresponding to the number of degenerate m_j states for the given value of j. (We note in passing that the figure orders the energies of the inner subshells in ascending fashion as

$$1s \quad 2s\,2p \quad 3s\,2p\,3d \quad \ldots .$$

This ordering of values of $E_{n\ell}$ holds for the *inner* electrons of a large-Z atom.) We note especially that the occurrence of the three split L subshells in Figure 9-12 is directly correlated with the existence of the three L absorption edges in Figure 9-10.

Let us now return to our picture of x-ray emission in Figure 9-9 and revise the diagrams to account for the splitting of the subshells. We illustrate the result in Figure 9-13 in terms of a particular x-ray transition. The indicated process shows the filling of an inner-shell hole by an electron from a higher subshell, along with the corresponding transition of the hole in the *opposite* direction. Since the initial and final states of the ion are associated with the location of the hole, it is conventional to represent the process as a *hole transition*. The convention employs an energy level diagram in which the highest energy state refers to a hole in the K shell, and in which the zero level refers to the ionic ground state where the hole occurs just beyond all the electron subshells. This presentation of the energy states of the ion *inverts* our view of the levels found in Figure 9-12 and produces an *x-ray level diagram* of the kind shown in Figure 9-14. The figure lists the values of the hole quantum numbers ($n\ell j$) and indicates the allowed hole transitions. These radiative processes are governed by the electric dipole selection rules, so that the single-particle quantum numbers are

Figure 9-14
X-ray levels of lead and transitions allowed by the electric dipole selection rules. The energies are plotted on a logarithmic scale.

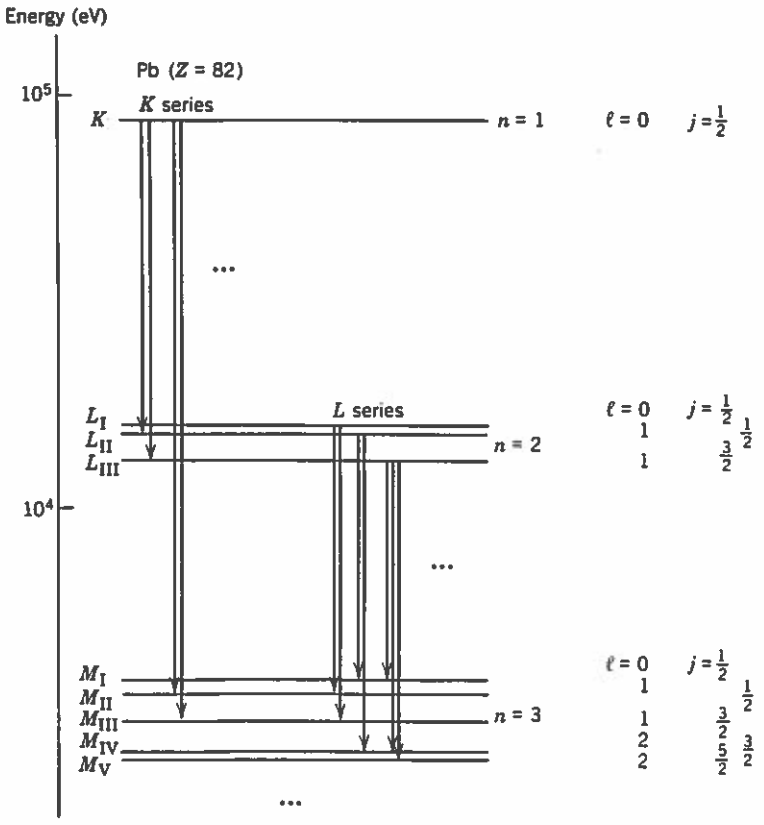

supposed to change according to the conditions

$$\Delta\ell = \pm 1 \quad \text{and} \quad \Delta j = 0 \text{ or } \pm 1 \quad (\text{but } 0 \not\to 0),$$

as in Equations (8-42) and (8-43). The various transitions are organized in the diagram into the different series of emission lines. We can employ this same general scheme whenever we wish to analyze the x-ray spectrum of any element.

Detail

We can formulate the spin–orbit interaction for an electron in a complex atom by constructing a parallel with the expression for the one-electron atom. Let us return to Equation (8-32) and rewrite the expression in terms of a derivative of the Coulomb potential energy:

$$V_{SL} = \frac{\mathbf{S}\cdot\mathbf{L}}{2m_e^2c^2}\frac{1}{r}\frac{dV}{dr},$$

where

$$V = -\frac{Ze^2}{4\pi\varepsilon_0 r} \quad \text{and} \quad \frac{1}{r}\frac{dV}{dr} = \frac{Ze^2}{4\pi\varepsilon_0 r^3}.$$

An electron in the central-field model has central potential energy $V_c(r)$, and so the spin–orbit interaction of the electron in the complex atom must have the form

$$V_{SL} = \mathbf{S}\cdot\mathbf{L}\xi_c(r)$$

in which

$$\xi_c(r) = \frac{1}{2m_e^2c^2}\frac{1}{r}\frac{dV_c}{dr}.$$

The function $V_c(r)$ contains the nuclear screening factor $Z_{\text{eff}}(r)$. This quantity varies between the value Z at small r and the value unity at large r, so that spin–orbit coupling becomes stronger with increasing Z, especially in states where r has a small average value. We know from Section 8-9 how the interaction V_{SL} perturbs the energy states in a central field. Let us consider an independent electron in an $n\ell$ subshell and describe the electron states by means of the quantum numbers $(n\ell jm_j)$ instead of the spin–orbital set $(n\ell m_\ell m_s)$. We use the eigenfunction $\psi_{n\ell jm_j}$ as before to calculate the expectation value of V_{SL}, and we obtain the following results:

$$\begin{aligned}\langle V_{SL}\rangle &= \left\langle \frac{J^2 - L^2 - S^2}{2}\xi_c(r)\right\rangle \\ &= \frac{\hbar^2}{2}\left[j(j+1) - \ell(\ell+1) - \frac{3}{4}\right]\langle\xi_c(r)\rangle \\ &= \frac{\hbar^2}{2}\langle\xi_c(r)\rangle\cdot\begin{cases}\ell & \text{for } j = \ell + \frac{1}{2} \\ -\ell - 1 & \text{for } j = -\ell - \frac{1}{2}.\end{cases}\end{aligned}$$

This energy shift affects the energy level of an electron in an $n\ell$ subshell according to the value of j and causes a splitting in every subshell with $\ell \neq 0$.

Example

The K and L_{III} absorption edges of lead in Figure 9-10 are observed at 0.01408 and 0.09511 nm. Let us consult Equation (9-13) and use these numbers to compute the wavelength emitted in the $K \rightarrow L_{III}$ transition:

$$\frac{1}{\lambda(KL_{III})} = \frac{1}{\lambda_K} - \frac{1}{\lambda_{L_{III}}} = \frac{1}{0.01408 \text{ nm}} - \frac{1}{0.09511 \text{ nm}} = \frac{1}{0.01653 \text{ nm}}.$$

This emission line can also be predicted from the energies of the K and L_{III} x-ray levels of lead. We use the tabulated values $E_K = 88.00$ keV and $E_{L_{III}} = 13.03$ keV, and we find

$$\lambda(KL_{III}) = \frac{hc}{E_K - E_{L_{III}}} = \frac{1.240 \text{ keV} \cdot \text{nm}}{74.97 \text{ keV}} = 0.01654 \text{ nm}.$$

Both calculations agree with the wavelength listed in the tables for the KL_{III} line of lead. The line and the transition are included among the information given in Figures 9-10 and 9-14.

9-5 Electron Antisymmetry

We have been able to implement the exclusion principle and explain the periodic table with only minimal use of quantum mechanics. The exclusion principle itself has been expressed in a limited context, based entirely on the assignment of electron quantum numbers in the central-field model. We now want to examine the fundamental quantum nature of Pauli's principle from the viewpoint of *electron indistinguishability* and develop the broader concept of *identical-particle symmetry*. We recall that we have already introduced this notion in the framework of one-dimensional quantum mechanics in Section 5-10.

Let us begin with the two-electron system and identify the degrees of freedom to be the pair of spatial coordinates and spin orientations

$$(\mathbf{r}_1, S_{1z}) \quad \text{and} \quad (\mathbf{r}_2, S_{2z}).$$

It is convenient to symbolize these variables in the wave function by adopting the abbreviated notation

$$\Psi(\mathbf{r}_1, S_{1z}, \mathbf{r}_2, S_{2z}, t) = \Psi(1, 2, t).$$

We then determine the probability of finding the two particles in two volume elements $d\tau_1$ and $d\tau_2$ at time t by evaluating the expression

$$|\Psi(1, 2, t)|^2 \, d\tau_1 d\tau_2.$$

The electrons in the system have identical physical attributes of charge $-e$, mass m_e, and spin $s = \frac{1}{2}$. It is not meaningful to refer to these particles as electron 1 and electron 2 because the notation implies that the two electrons can always be distinguished in any state. The intrinsic indistinguishability of identical quantum par-